Gating mechanisms of a natural anion channelrhodopsin

Oleg A. Sineshchekov, Elena G. Govorunova, Hai Li, and John L. Spudich[1]

Center for Membrane Biology, Department of Biochemistry and Molecular Biology, The University of Texas Health Science Center at Houston, Medical School, Houston, TX 77030

Edited by Peter H. Quail, University of California, Berkeley, Albany, CA, and approved September 28, 2015 (received for review July 10, 2015)

Anion channelrhodopsins (ACRs) are a class of light-gated channels recently identified in cryptophyte algae that provide unprecedented fast and powerful hyperpolarizing tools for optogenetics. Analysis of photocurrents generated by *Guillardia theta* ACR 1 (*Gt*ACR1) and its mutants in response to laser flashes showed that *Gt*ACR1 gating comprises two separate mechanisms with opposite dependencies on the membrane voltage and pH and involving different amino acid residues. The first mechanism, characterized by slow opening and fast closing of the channel, is regulated by Glu-68. Neutralization of this residue (the E68Q mutation) specifically suppressed this first mechanism, but did not eliminate it completely at high pH. Our data indicate the involvement of another, yet-unidentified pH-sensitive group X. Introducing a positive charge at the Glu-68 site (the E68R mutation) inverted the channel gating so that it was open in the dark and closed in the light, without altering its ion selectivity. The second mechanism, characterized by fast opening and slow closing of the channel, was not substantially affected by the E68Q mutation, but was controlled by Cys-102. The C102A mutation reduced the rate of channel closing by the second mechanism by ∼100-fold, whereas it had only a twofold effect on the rate of the first. The results show that anion conductance by ACRs has a fundamentally different structural basis than the relatively well studied conductance by cation channelrhodopsins (CCRs), not attributable to simply a modification of the CCR selectivity filter.

ion transport | channel gating | channelrhodopsins | optogenetics

Recently we reported a class of rhodopsins from the cryptophyte alga *Guillardia theta* that act as anion-conducting channels when expressed in cultured animal cells and therefore can be used to suppress neuronal firing by light (1). These proteins—named anion channelrhodopsins (ACRs)—show distant sequence homology to cation channelrhodopsins (CCRs) from chlorophyte (green) algae (2), but completely lack permeability for protons and metal cations. This property, as well as large current amplitudes and fast kinetics, makes ACRs superior hyperpolarizing optogenetic tools, compared with proton and chloride pumps (3, 4), or engineered Cl^--conducting CCR variants (5, 6). Two *G. theta* (*Gt*) ACRs differ in their spectral sensitivity and channel kinetics (1). *Gt*ACR1, with its absorption peak at 515 nm (Fig. S1), has an advantage over a more blue-shifted *Gt*ACR2 with maximal efficiency at 470 nm, because it allows using light of longer wavelengths that is less scattered by biological tissue.

Because a CCR could be altered to exhibit Cl^- channel activity by mutation of a single amino acid residue (5), a fundamental question about ACRs is whether they differ from CCRs only by their selectivity filter. In our search for an answer, we analyzed photocurrents generated by *Gt*ACR1 in HEK293 cells under single-turnover conditions in which secondary photochemistry does not complicate the photocycle. We found that *Gt*ACR1 conductance comprises two distinct mechanisms with opposite dependencies on the membrane voltage and bath pH, but the same ionic selectivity. The first mechanism, observed by a fast component of the photocurrent decay, depends on Glu-68, the position occupied by a positively charged residue in the engineered Cl^--conducting CCR mutant. Substitution of Glu-68 with Arg in *Gt*ACR1 did not change anion selectivity of the channel, but, rather, inverted its gating, rendering it constitutively open in the dark and closed in the light. The second mechanism, reflected by a slow component of the current decay, involves Cys-102. Our results demonstrate that the structural basis for anion conductance in ACRs is fundamentally different from that of Cl^--conducting CCR mutants.

Results

The rise and decay of photocurrents generated by *Gt*ACR1 response to a 6-ns laser flash under our standard ionic conditions (150 mM NaCl in the bath and 126 mM KCl in the pipette, pH 7.4; for other components, see *SI Materials and Methods*) were both at least biphasic (Fig. 1*A*). Exponential functions were fit to the data to derive amplitudes and time constants (τ) of each component. At the holding voltage (E_h) −60 mV, τ of the major rise component (∼95%) was 86 ± 15 μs, accompanied by a minor component with τ 1.8 ± 0.3 ms (mean ± SEM; $n = 5$). In some cases, this minor rise component could be further deconvoluted in two, but this additional complexity was not addressed in the present study. The two decay components had comparable amplitudes and τ values of 48 ± 2 ms and 245 ± 20 ms (mean ± SEM; $n = 5$). A third, very slow decay component could also be resolved, but its contribution was ≤0.5% and was not considered here.

Previously we reported that the voltage dependence of the peak *Gt*ACR1 current recorded in response to a pulse of continuous light is linear (1), in contrast to inward rectification typical of the current–voltage relationships of CCRs (7). Deconvolution of laser-flash–evoked currents revealed that the voltage dependence of the amplitude of the fast decay showed outward rectification,

Significance

The recently discovered natural anion channelrhodopsins (ACRs) have exceptional properties for use as membrane-hyperpolarizing tools for neural silencing, but our knowledge about them is only rudimentary. We have gained, to our knowledge, first insights into the molecular mechanisms of their unique light-gated anion conductance by photocurrent measurements and mutant analysis. We identified a mutant constitutively open in the dark—to our knowledge, the first such mutant of any light-gated channel, invaluable for probing the structure of the channel open state—and a "step function" ACR mutant useful in some optogenetics protocols. Our results will help decipher the mechanism of channelrhodopsin ion conductance and facilitate rational design of inhibitory tools tailored to the needs of optogenetic studies and potential clinical applications.

Author contributions: O.A.S., E.G.G., and J.L.S. designed research; O.A.S., E.G.G., and H.L. performed research; O.A.S., E.G.G., and J.L.S. analyzed data; and O.A.S., E.G.G., and J.L.S. wrote the paper.

The authors declare no conflict of interest.

This article is a PNAS Direct Submission.

[1]To whom correspondence should be addressed. Email: john.l.spudich@uth.tmc.edu.

This article contains supporting information online at www.pnas.org/lookup/suppl/doi:10.1073/pnas.1513602112/-/DCSupplemental.

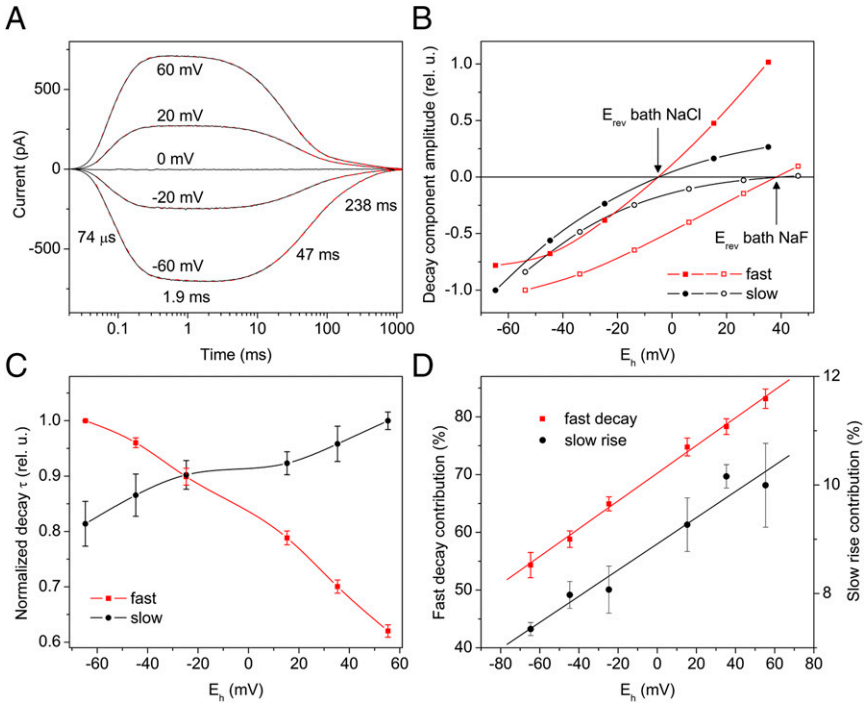

Fig. 1. The voltage dependence of the kinetic components of the current. (*A*) Typical photocurrents generated by *Gt*ACR1 in a HEK293 cell in response to a laser flash (6 ns, 532 nm) at the holding voltages (E_h) indicated. Ten individual sweeps recorded with 5-s intervals at each E_h were averaged, smoothed by logarithmic adjacent averaging, and fit with four exponential functions to derive the time constants (τ) shown for the trace recorded at −60 mV in this particular cell. For mean τ values for an ensemble of cells, see text. The experimental data are shown as black solid lines and the fitted curves as red dashed lines. (*B*) The voltage dependence of the amplitudes of the two decay components determined by exponential fit as shown in *A*, measured in a typical cell in the standard bath solution (filled symbols) and upon substitution of F^- for Cl^- (open symbols). (*C*) The voltage dependence of τ values of the two decay components. The data points are mean values ± SEM ($n = 14$). (*D*) The voltage dependence of the contributions of the fast decay (left axis) and slow rise (right axis) to the total amplitude. The data points are mean values ± SEM ($n = 9$).

whereas that of the slow component showed inward rectification (Fig. 1*B*). The fast decay phase strongly accelerated upon shifting E_h to more positive values, but the slow phase became even slower (Fig. 1*C*). The rates of the two components of the rise were nearly voltage-independent (Fig. S2*A*). However, the contribution of the slow rise component to the total amplitude increased at more positive voltages, as did that of the fast decay (Fig. 1*D*). These results indicate that *Gt*ACR1 channel conductance comprises two mechanisms, one with the slow rise and fast decay and another with the fast rise and slow decay, which are altered in opposite way by changes in membrane voltage. The biphasic rise and decay cannot be explained by two preexisting populations of *Gt*ACR1 undergoing different photocycles, because the relative contributions of the rise components do not match those of the corresponding decay components (Fig. 1*D*). We measured the action spectra of photocurrents under conditions that dramatically alter relative contribution of the two gating mechanisms. Within the accuracy of our measurements, the spectral sensitivity did not depend on the voltage, the bath pH, or even on a mutation of the key residue (see below) that controls fast channel closing (Fig. S1). These findings confirm the absence of spectrally identifiable heterogeneity of the unphotolyzed state of *Gt*ACR1.

The two conducting forms have the same relative permeability for Cl^-: When Cl^- in the bath was replaced with F^-, the current–voltage relationships for the amplitudes of both decay components shifted to the same extent (Fig. 1*B*, open symbols). However, replacement of Cl^- in the bath with F^- or Asp^- strongly accelerated the fast current decay (Fig. S3), whereas the slow decay was not changed. A similar acceleration of closure when F^- ions pass through the channel has been observed in neuronal gamma-aminobutyric acid (GABA)-activated chloride channels (8).

The two conducting forms of *Gt*ACR1 also showed opposite dependencies on the bath pH. The fast decay strongly accelerated (Fig. 2*A* and black filled symbols in Fig. 2*B*), whereas the slow decay was much less sensitive and slowed upon an increase in bath pH (Fig. S2*B*).

The fast decay rate was nearly completely insensitive to the intracellular pH (Fig. 2*B*, black open symbols), whereas it exhibited a strong dependence on the extracellular pH with a pK_a ~9.7 (Fig. 2*B*, black filled symbols). Therefore, we hypothesized that deprotonation of a specific amino acid residue accessible from the extracellular side of the membrane is required for fast channel closing in *Gt*ACR1. Although the pK_a values of the Asp and Glu side chains in solution are much lower than 9.7, it is known that the protein environment can significantly increase them (9). Therefore, we started a mutagenesis scan for this critical residue by individually substituting Asn for Asp and Gln for Glu in the transmembrane domain of *Gt*ACR1. The positions of the mutated residues in our *Gt*ACR1 homology model are shown in Fig. S4. Glu-60 was also included in this analysis, although its predicted location is close to the cytoplasmic surface, because this position corresponds to Glu-82 of *Chlamydomonas reinhardtii* channelrhodopsin 2 (*Cr*ChR2), in which its replacement with Ala strongly inhibited photocurrents (10). All but one tested *Gt*ACR1 mutant exhibited biphasic current rise and decay, as did wild type (WT), although the rates and contributions of the phases to the total amplitude quantitatively varied (Fig. S5).

In contrast, both the rise and decay of photocurrents recorded at the bath pH 7.4 from the *Gt*ACR1_E68Q mutant were monoexponential (Fig. 3*A*, red line). At higher pH values, however, a biphasic current rise and decay were observed also in this mutant (Fig. 3*A*, blue line). The contributions of fast-closing and slow-opening components in the mutant strongly diminished in parallel

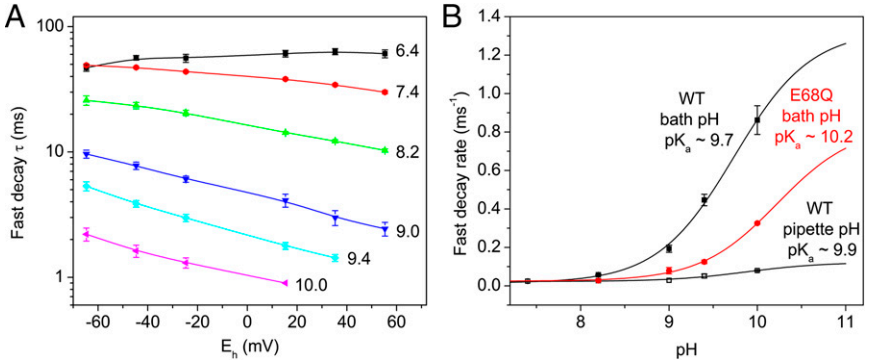

Fig. 2. The influence of pH on the fast current decay. (*A*) The voltage dependence of the fast decay τ at the indicated pH of the bath. The data points are mean values ± SEM (n = 4–10 cells). (*B*) The dependence of the fast decay rate measured at 0 mV on the pH of the bath (filled symbols, black for WT and red for the E68Q mutant) and the pipette (black open symbols, WT). The data points are mean values ± SEM (n = 4–10 cells).

until vanishing upon a decrease in pH (Fig. 3*B*, circles and solid lines). Therefore, the remaining monoexponential opening and closing of the channel observed in the mutant at neutral pH corresponds to the fast rise/slow decay gating mechanism in WT. The rate of fast decay in the mutant was severalfold slower (Fig. 2*B*, red symbols) than in WT at the same pH. The pH dependence of the slow decay rate was similarly weak as in WT, but changed in the opposite direction (Fig. 3*B*, squares and dashed line). The suppression of the fast decay component by E68Q mutation was also strongly supported by measurements in the double E68Q_C102A mutant (see below). Our interpretation of these results is that, in addition to the Glu-68 residue, fast closing of the channel involves another yet unidentified pH-sensitive group X. The E68Q mutation led to a substantial suppression of the gating mechanism associated with the slow opening/fast closing of the channel. However, this mutation did not influence the current amplitude (Fig. S6*A*) and anion permeability of *Gt*ACR1: The E_{rev} of photocurrents recorded from the mutant were close to that of WT in both the standard bath solution and upon replacement of Cl^- with F^- (Fig. S6*B*).

To test the effect of a positive charge in the Glu-68 position, we replaced it with Arg. The *Gt*ACR1_E68R mutant demonstrated a unique "inverted" behavior, which is best illustrated by application of a continuous light pulse: Illumination caused currents to change in the opposite direction than that observed in any thus-far-tested ChRs (Fig. 4*A*). This behavior implies that switching on the light caused a decrease, rather than an increase in *Gt*ACR1_E68R conductance—i.e., the *Gt*ACR1_E68R channel is constitutively open in the dark and closes upon illumination.

To further test this interpretation, we measured current–voltage relationships (*IE* curves) and compared E_{rev} shifts observed upon substitution of poorly permeable F^- or nonpermeable Asp^- for Cl^- in the bath for the WT *Gt*ACR1 and its E68R mutant. First, we analyzed current responses to voltage steps applied in the dark. As expected of leak currents, in the WT, the *IE* curves were linear and insensitive to the bath exchange. In contrast, the *IE* curves in the mutant changed their shape and shifted to more positive voltages upon the bath exchange (Fig. 4*B* and black solid bars in Fig. 4*C*), which showed that in the mutant, a specific anion conductance was present in the dark, as expected from an open *Gt*ACR1_E68R channel.

Next, we examined the behavior of the *IE* curves in response to illumination. In the WT, illumination caused a positive shift of the E_{rev}, which was greater for nonpermeable Asp^- in the bath than for poorly permeable F^- (Fig. 4*C*, red hatched bars), as expected (1). In other words, illumination caused the appearance of Cl^- conductance in the WT (channel opening). In contrast, in the mutant illumination caused a negative shift of E_{rev} shift with either F^- or Asp^-, indicating closing of Cl^- channels (Fig. 4*C*, red solid bars).

Photocurrents from the E68R mutant elicited by a laser flash could be fit with only three exponentials (two for the rise—i.e., closing of the channel—and one for the decay—i.e., reopening of the channel; Fig. 4*D*), but a better fit was obtained when the slower rise component was split into two components. The E_{rev}

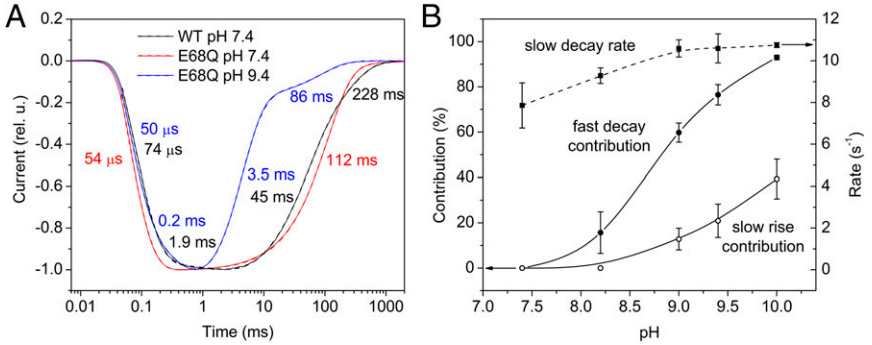

Fig. 3. (*A*) Typical photocurrents generated at −60 mV by the *Gt*ACR1_E68Q mutant at the bath pH 7.4 (solid red line) and 9.4 (solid blue line). The current traces were normalized at the peak value and fit with multiexponential functions (dashed lines) that yielded the indicated τ values for the current rise and decay. The normalized WT current from Fig. 1*A* was fitted with four exponentials (black lines), and its τ values are shown for comparison. (*B*) The influence of the bath pH on the slow rise (open circles) and fast decay (filled circles) contribution (left axis) and the slow decay rate (filled squares; right axis) in the *Gt*ACR1_E68Q mutant. The data points are mean values ± SEM (n = 3–5 cells).

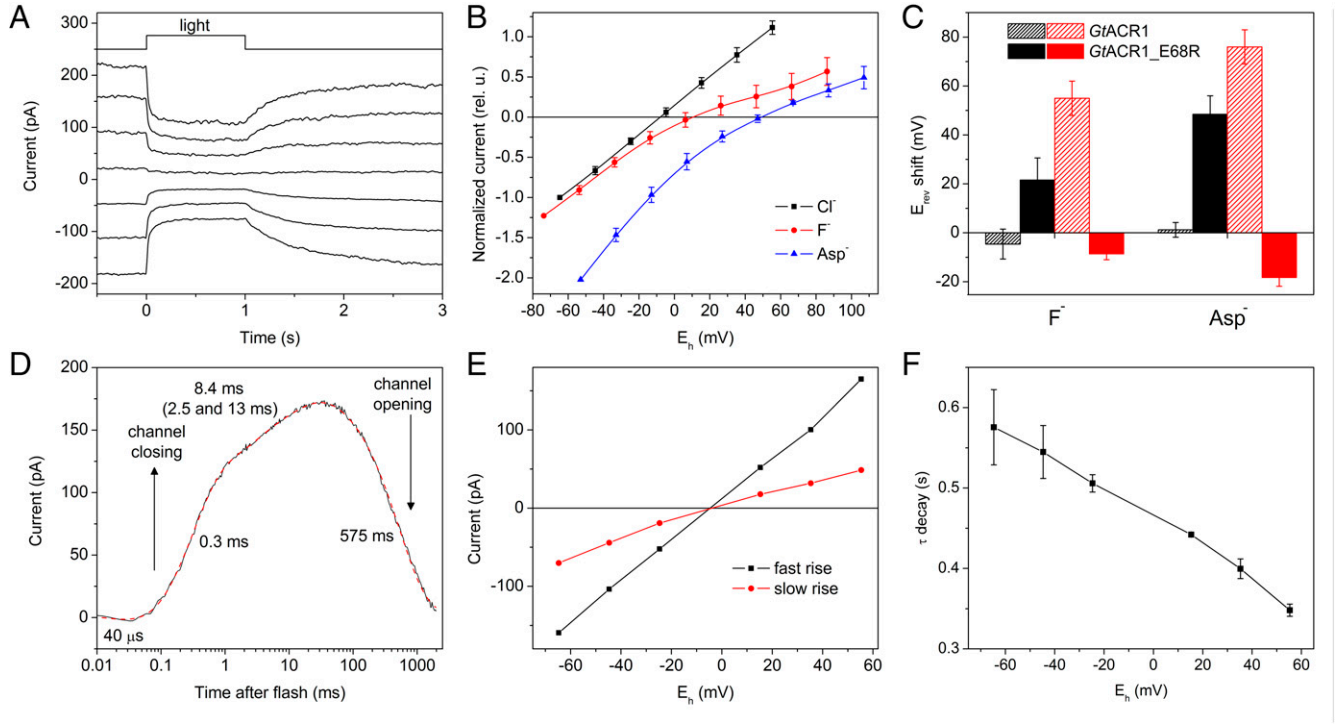

Fig. 4. Photocurrents from the inverted *Gt*ACR1_E68R mutant. (*A*) Typical photocurrents generated in response to a 1-s light pulse by the *Gt*ACR1_E68R mutant in a HEK293 cell at voltages from −60 mV (bottom trace) to 60 mV (top trace) changed in 20-mV steps. (*B*) The current–voltage relationships measured in the *Gt*ACR1_E68R mutant in the dark. The data are mean values ± SEM ($n = 3$ or 4 cells) normalized to the value measured at −60 mV in the standard (Cl^-) bath. (*C*) The E_{rev} shifts measured for currents generated by WT *Gt*ACR1 and the *Gt*ACR1_E68R mutant in the dark upon switching from the standard (Cl^-) bath solution to that with F^- or Asp^- (black bars) and upon illumination in the same indicated bath (red bars). The data points are mean values ± SEM ($n = 3$ or 4 cells). (*D*) A typical photocurrent trace generated by *Gt*ACR1_E68R in response to a laser flash at −60 mV (solid line). The dark current level was subtracted. The red dashed line is a multiexponential fit of the signal yielding indicated τ values. (*E*) The voltage dependencies of the amplitudes of the rise (channel closure) components of the laser-evoked signals generated by *Gt*ACR1_E68R in a typical cell. (*F*) The voltage dependence of the decay τ values of the laser-evoked signals. The data points are mean values ± SEM ($n = 3$ cells).

of both rise components was the same (Fig. 4*E*). All current components accelerated upon the membrane depolarization, but the decay was most sensitive to it (Fig. 4*F*). The light-induced closing of the channel (the current rise) was preceded by a fast (τ ~40 µs) negative component, the amplitude of which varied from cell to cell. Although its nature is not yet clear, it may reflect a fast electrical response related to retinal isomerization.

Cys-102 in *Gt*ACR1 corresponds to Cys-128 in *Cr*ChR2, the mutation of which leads to a dramatic decrease of the current decay rate [so-called step-function tools (11)]. In the *Gt*ACR1_C102A mutant, the fast current decay (30% contribution) was only twofold slower (τ 91 ± 2 ms; $n = 5$ cells) than that in the WT, indicating that Cys-102 was relatively unimportant for the fast decay conductance mechanism (Fig. 5, red line). In contrast, the slow decay in this mutant was dramatically slower than that in the WT and comprised two phases with 38% and 32% contributions and τ values 7.5 ± 0.9 and 53 ± 9 s, respectively ($n = 5$ cells). In the double mutant *Gt*ACR1_E68Q_C102A, the contribution of the fast current decay was reduced approximately fourfold, and its rate slowed compared with the single C102A mutant (Fig. 5, green line). This result further confirms that Glu-68 is a key residue that controls fast channel closing.

Cys-128 in *Cr*ChR2 has been proposed to form a hydrogen bond with Asp-156 in the fourth transmembrane helix [the so-called "DC" gate (12)]. The corresponding residue in *Gt*ACR1 is Ser-130, which, according to our homology model, is predicted to form a hydrogen bond with Cys-102 (Fig. S4). However, replacement of Ser-130 with Ala did not greatly influence the rate of channel closing, with that of both phases becoming only ~50% reduced in the mutant (Fig. 5, blue line) compared with the WT, in a striking contrast to the effect of the corresponding D156A mutation in *Cr*ChR2 (13).

Discussion

We show that both rise and decay of photocurrents generated by *Gt*ACR1 upon excitation with short laser flashes (single-turnover conditions) proceed in two phases. Qualitative analysis of the dependencies of these phases on the membrane voltage and the external pH suggests that *Gt*ACR1 exhibits two conduction-gating mechanisms. One of these mechanisms is characterized by a fast rise and slow decay, and the other one by a slow rise and fast decay. Our observations raise two possibilities: (*i*) The same anion gate is controlled by two distinct mechanisms—i.e., there are two different ways to remove the structural block defining the gate. (*ii*) The anion channel diverges into two branches, each with its own gate, so that if either gate opens, the ions can flow. Distinguishing these possibilities will likely require structural analysis of ACRs and their mutants altered in gating properties.

Selective influence of specific mutations on each of the two components of the photocurrent decay strongly supports the existence of two distinct gating mechanisms of *Gt*ACR1. We have identified Glu-68 in the second transmembrane helix of *Gt*ACR1 as an essential residue that controls the slow rise/fast decay mechanism, most probably by a protonation change. In contrast, the E68Q mutation has essentially no effect on the fast rise/slow decay mechanism. According to the primary sequence alignment, Glu-68 corresponds to Glu-90, the residue that determines cation selectivity of *Cr*ChR2 (7, 14, 15). Mutation of Glu-90 to Lys or Arg converted *Cr*ChR2 to an anion channel with residual permeability for protons (5). However, the selectivity filter of ACRs appears to

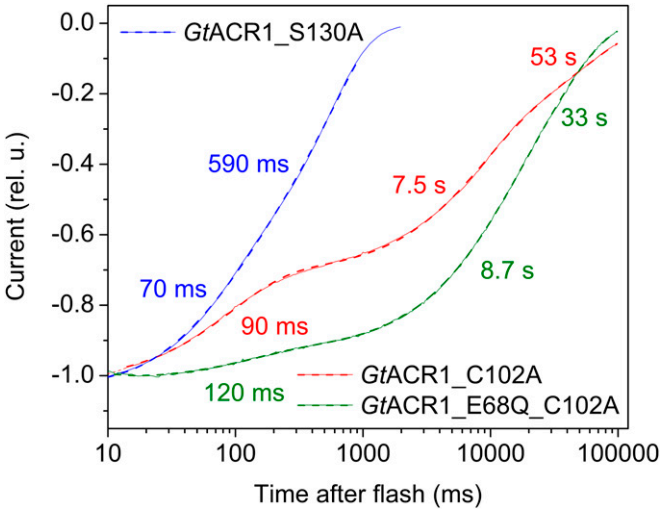

Fig. 5. The decay of typical photocurrents generated by *Gt*ACR1_C102A (solid red line), *Gt*ACR1_E68Q_C102A (solid green line), and *Gt*ACR1_S130A (solid blue line) at −60 mV in the standard bath solution. The traces were normalized at the peak amplitude. The corresponding dashed lines show two- or three-exponential fits used to determine the decay time constants for the mutants, as shown on the graph.

be different from that of the *Cr*ChR2_E90K/R mutants, because the presence of the Glu-90 homolog in WT *Gt*ACRs is obviously not a barrier to anion permeation. Furthermore, replacement of Glu-68 with Gln or Arg in *Gt*ACR1 did not change anion permeability of the channel, which confirmed that this residue does not determine the selectivity filter in ACRs.

Although the E68R mutation did not change the ionic selectivity of the channel, it inverted its gating. The channel became constitutively open in the dark, whereas illumination caused it to close. A similar inversion of protein function was previously observed in haloarchaeal sensory rhodopsin I (SRI), in which a single point mutation either of the photoreceptor itself or of its cognate transducer converted SRI from an attractant to a repellent photoreceptor (16, 17). The SRI inversion is attributable to a switch in its conformation from the C (retinylidene Schiff base accessible from the cytoplasm) to E (Schiff base accessible from the extracellular space) conformer (18–20). The stable open channel of GtACR1_E68R is likely to be particularly valuable for structural comparisons with the WT by enabling identification of residue determinants and structural changes distinguishing the closed and open conformations of the channel by structural methods such as molecular spectroscopy and crystallography.

Our mutant analysis showed that Cys-102 controls only the slow phase of the photocurrent decay, corresponding to the fast opening/slow closing gate, whereas its fast decay phase was practically unaffected by the *Gt*ACR1_C102A mutation. This residue (Cys-128 in *Cr*ChR2) is conserved in all thus-far-known ACRs and CCRs, but is substituted with Val in the third homologous sequence from *G. theta* that generated no photocurrents, despite good expression in HEK293 cells (1). The effects of C128X mutations on channel activity have been best studied in *Cr*ChR2 (11, 13), but a similar dramatic decrease in the current decay rate was also observed in the corresponding mutants of other CCRs, such as *Mesostigma viride* channelrhodopsin 1 (*Mv*ChR1) (21). This result has been attributed to a disruption of the hydrogen bond ("DC gate") that Cys-128 forms with Asp-156 in *Cr*ChR2 (12). Indeed, mutation of Asp-156 yielded comparable or even greater extension of the channel open time, as did that of Cys-128 (13, 22). In *Gt*ACR1, the position of Asp-156 is occupied by Ser-130, which, according to our homology model, forms a hydrogen bond with Cys-102. However, in the S130A mutant, the slow decay phase was practically unchanged, which suggests that the effect of the C102A mutation in *Gt*ACR1 was not caused by a disruption of the putative hydrogen bond.

The two gating mechanisms of *Gt*ACR1 identified by kinetic analysis of laser-evoked signals control conduction with the same anion selectivity. None of the tested mutations that selectively influenced the kinetics of each form changed anion selectivity of *Gt*ACR1. These observations show that in *Gt*ACR1 channel gating is structurally independent of the selectivity filter. In contrast, in *Cr*ChR2 two conducting states have been recognized by their different relative permeability to H^+ and Na^+ (23, 24). A model of two interconnected photocycles, each of which contains a closed (nonconducting) state and an open (conducting) state, has been developed for CCRs (25–27). However, single-turnover photocurrents generated by *Cr*ChR2 upon laser excitation decay monoexponentially (28, 29), which means that the second conducting state accumulates only under continuous light, indicating that the second state requires secondary photochemistry. Two exponential phases have been resolved in the decay of laser-evoked photocurrents from the *Volvox carteri* channelrhodopsin 1/*Volvox carteri* channelrhodopsin 2 (*Vc*ChR1/*Vc*ChR2) hybrid (30), but this phenomenon has not yet been incorporated into the four-state model.

The importance of the Cys-128 homolog is not the only similarity between the slow phase of the decay of *Gt*ACR1 photocurrent and the monoexponential decay of the current generated by *Cr*ChR2. The latter also became slower with membrane depolarization (29, 31). However, in *Cr*ChR2, this voltage dependence was eliminated by the E123T mutation (29), whereas in WT *Gt*ACR1, the voltage dependence persisted in the presence of a noncarboxylic residue (Ser-97) in the position of Glu-123 (corresponding to Asp-85 in bacteriorhodopsin).

The many differences between ACR and CCR conductance mechanisms evident in our results clearly indicate that ACRs differ from CCRs, not simply by their selectivity filter, but they represent a distinct class of light-gated channels that evolved to conduct anions.

Materials and Methods

A DNA polynucleotide encoding the seven-transmembrane domain (residues 1–295) of *Gt*ACR1 optimized for human codon use was synthesized and mutated as described in *SI Materials and Methods*. Photocurrents were evoked by a Nd:YAG laser (532 nm, pulsewidth 6 ns) and recorded by whole-cell patch clamp from HEK293 cells transiently transfected with WT *Gt*ACR1 or its mutants fused to enhanced YFP. A laser artifact measured with a blocked optical path was digitally subtracted from the recorded traces. For further analysis, the signals were logarithmically averaged with a custom-created computer algorithm. For multiexponential curve fitting, Origin 7 software was used. Monochromatic (10 nm half-band) light from a Polychrome IV light source was used in experiments with continuous light pulses. All current–voltage dependencies were corrected for liquid junction potentials (LJPs) calculated by using the ClampEx built-in LJP calculator. Action spectra were constructed by correction of measured currents for quantum density of the stimulation light. *SI Materials and Methods* provides detailed description of experimental procedures.

ACKNOWLEDGMENTS. This work was supported by NIH Grant R01GM027750, the Hermann Eye Fund, and Endowed Chair AU-0009 from the Robert A. Welch Foundation.

1. Govorunova EG, Sineshchekov OA, Janz R, Liu X, Spudich JL (2015) Natural light-gated anion channels: A family of microbial rhodopsins for advanced optogenetics. *Science* 349(6248):647–650.
2. Nagel G, et al. (2005) Channelrhodopsins: Directly light-gated cation channels. *Biochem Soc Trans* 33(Pt 4):863–866.
3. Gradinaru V, Thompson KR, Deisseroth K (2008) eNpHR: A *Natronomonas* halorhodopsin enhanced for optogenetic applications. *Brain Cell Biol* 36(1-4): 129–139.
4. Chow BY, et al. (2010) High-performance genetically targetable optical neural silencing by light-driven proton pumps. *Nature* 463(7277):98–102.

5. Wietek J, et al. (2014) Conversion of channelrhodopsin into a light-gated chloride channel. *Science* 344(6182):409–412.
6. Berndt A, Lee SY, Ramakrishnan C, Deisseroth K (2014) Structure-guided transformation of channelrhodopsin into a light-activated chloride channel. *Science* 344(6182):420–424.
7. Gradmann D, Berndt A, Schneider F, Hegemann P (2011) Rectification of the channelrhodopsin early conductance. *Biophys J* 101(5):1057–1068.
8. Robertson B (1989) Characteristics of GABA-activated chloride channels in mammalian dorsal root ganglion neurones. *J Physiol* 411:285–300.
9. Li H, Govorunova EG, Sineshchekov OA, Spudich JL (2014) Role of a helix B lysine residue in the photoactive site in channelrhodopsins. *Biophys J* 106(8):1607–1617.
10. Sugiyama Y, et al. (2009) Photocurrent attenuation by a single polar-to-nonpolar point mutation of channelrhodopsin-2. *Photochem Photobiol Sci* 8(3):328–336.
11. Berndt A, Yizhar O, Gunaydin LA, Hegemann P, Deisseroth K (2009) Bi-stable neural state switches. *Nat Neurosci* 12(2):229–234.
12. Nack M, et al. (2010) The DC gate in Channelrhodopsin-2: Crucial hydrogen bonding interaction between C128 and D156. *Photochem Photobiol Sci* 9(2):194–198.
13. Bamann C, Gueta R, Kleinlogel S, Nagel G, Bamberg E (2010) Structural guidance of the photocycle of channelrhodopsin-2 by an interhelical hydrogen bond. *Biochemistry* 49(2):267–278.
14. Ruffert K, et al. (2011) Glutamate residue 90 in the predicted transmembrane domain 2 is crucial for cation flux through channelrhodopsin 2. *Biochem Biophys Res Commun* 410(4):737–743.
15. Eisenhauer K, et al. (2012) In channelrhodopsin-2 Glu-90 is crucial for ion selectivity and is deprotonated during the photocycle. *J Biol Chem* 287(9):6904–6911.
16. Olson KD, Zhang XN, Spudich JL (1995) Residue replacements of buried aspartyl and related residues in sensory rhodopsin I: D201N produces inverted phototaxis signals. *Proc Natl Acad Sci USA* 92(8):3185–3189.
17. Jung KH, Spudich JL (1998) Suppressor mutation analysis of the sensory rhodopsin I-transducer complex: Insights into the color-sensing mechanism. *J Bacteriol* 180(8): 2033–2042.
18. Sineshchekov OA, Sasaki J, Phillips BJ, Spudich JL (2008) A Schiff base connectivity switch in sensory rhodopsin signaling. *Proc Natl Acad Sci USA* 105(42):16159–16164.
19. Sineshchekov OA, Sasaki J, Wang J, Spudich JL (2010) Attractant and repellent signaling conformers of sensory rhodopsin-transducer complexes. *Biochemistry* 49(31): 6696–6704.
20. Sasaki J, Takahashi H, Furutani Y, Kandori H, Spudich JL (2011) Sensory rhodopsin-I as a bidirectional switch: Opposite conformational changes from the same photoisomerization. *Biophys J* 100(9):2178–2183.
21. Govorunova EG, Spudich EN, Lane CE, Sineshchekov OA, Spudich JL (2011) New channelrhodopsin with a red-shifted spectrum and rapid kinetics from *Mesostigma viride*. *MBio* 2(3):e00115-11.
22. Dawydow A, et al. (2014) Channelrhodopsin-2-XXL, a powerful optogenetic tool for low-light applications. *Proc Natl Acad Sci USA* 111(38):13972–13977.
23. Berndt A, Prigge M, Gradmann D, Hegemann P (2010) Two open states with progressive proton selectivities in the branched channelrhodopsin-2 photocycle. *Biophys J* 98(5):753–761.
24. Schneider F, Gradmann D, Hegemann P (2013) Ion selectivity and competition in channelrhodopsins. *Biophys J* 105(1):91–100.
25. Hegemann P, Ehlenbeck S, Gradmann D (2005) Multiple photocycles of channelrhodopsin. *Biophys J* 89(6):3911–3918.
26. Nikolic K, et al. (2009) Photocycles of channelrhodopsin-2. *Photochem Photobiol* 85(1): 400–411.
27. Stehfest K, Hegemann P (2010) Evolution of the channelrhodopsin photocycle model. *ChemPhysChem* 11(6):1120–1126.
28. Tsunoda SP, Hegemann P (2009) Glu 87 of channelrhodopsin-1 causes pH-dependent color tuning and fast photocurrent inactivation. *Photochem Photobiol* 85(2):564–569.
29. Berndt A, et al. (2011) High-efficiency channelrhodopsins for fast neuronal stimulation at low light levels. *Proc Natl Acad Sci USA* 108(18):7595–7600.
30. Ernst OP, et al. (2008) Photoactivation of channelrhodopsin. *J Biol Chem* 283(3): 1637–1643.
31. Bamann C, Kirsch T, Nagel G, Bamberg E (2008) Spectral characteristics of the photocycle of channelrhodopsin-2 and its implication for channel function. *J Mol Biol* 375(3):686–694.